DEVELOPMENT OF DETAILED CHEMISTRY MODELS FOR BOUNDARY LAYER CATALYTIC RECOMBINATION

G. Bellas-Chatzigeorgis[1,2], P. F. Barbante[3], and T. E. Magin[4]

[1]*Politecnico di Milano, Department of Mathematics, P.zza Leonardo da Vinci 32, 20133 Milano, Italy*
[2]*von Karman Institute for Fluid Dynamics, Aeronautics and Aerospace Department, Chaussée de Waterloo 72, 1640 Rhode-Saint-Genèse, Belgium, Email: georgios.bellas.chatzigeorgis@vki.ac.be*
[3]*Politecnico di Milano, MOX, Department of Mathematics, P.zza Leonardo da Vinci 32, 20133 Milano, Italy, Email: paolo.barbante@polimi.it*
[4]*von Karman Institute for Fluid Dynamics, Aeronautics and Aerospace Department, Chaussée de Waterloo 72, 1640 Rhode-Saint-Genèse, Belgium, Email: thierry.magin@vki.ac.be*

ABSTRACT

During the (re-)entry phase of a space vehicle, the gas flow in the shock layer can be in a state of strong thermal non-equilibrium. Under these circumstances, the population of the internal energy levels of the atoms and molecules of the gas deviates from the Boltzmann distribution. A substantial increase of the heat flux transferred from the gas to the vehicle is possible, as the thermal protection system of the vehicle acts as a catalyzer. The objective of the paper is to show how thermal non-equilibrium and catalysis can jointly influence wall heat flux predictions. In order to study thermal non-equilibrium effects a coarse-grained State-to-State model for nitrogen is used coupled with a phenomenological model for catalysis. From the numerical simulations performed, an important effect on the heat flux has been observed due to the interaction of catalysis and thermal non-equilibrium at the wall.

Key words: catalysis, gamma model, state-to-state models, thermal non-equilibrium, accommodation coefficient, stagnation line.

1. INTRODUCTION

The design of the thermal protection system for a spaceship during an atmospheric entry is a very challenging task due to the multi-physics phenomena occurring in the shock layer of the space vehicle [1]. These phenomena include strong deviation from thermochemical equilibrium [22], radiative heating [17] and gas-surface interaction (catalysis and ablation) between the vehicle's surface and the surrounding gas [6]. These phenomena are strongly coupled between each other and this makes the prediction of the flow-field properties very difficult. Currently, most researchers try to deal with each of these phenomena separately or with simplified coupling strategies. For a relevant fraction of the re-entry trajectory the flow-field behind the shock wave and in the boundary layer is in a state of thermal non-equilibrium; the populations of the internal energy levels of atoms and molecules deviates from the Boltzmann distribution. A substantial increase in the heat flux can observed as the catalycity of the wall of a re-entry vehicle increases with wall temperature [5, 26]. Currently, most of the simulations performed by the community assume thermal equilibrium in the flow field. The objective of this contribution is to study the joint effect of thermal non-equilibrium and catalysis on the predicted heat flux.

2. PHYSICAL MODEL

Thermal non-equilibrium is studied with a state-to-state rovibrational specific nitrogen model developed by the NASA Ames Research Center [12]. The model can simulate flows that depart from Boltzmann equilibrium, like strongly compressing, expanding and boundary layer flows [21]. Each internal energy level is assumed to be a distinct pseudo species. Chemical reactions are the mechanisms responsible for transforming one of these pseudo species to another one. Even though state-to-state models are more accurate than multi-temperature ones, they lead to a drastic increase of the computational cost. A possible strategy to reduce the the computational cost is presented in the paper.

2.1. Energy Levels

The nitrogen model has 9390 different rovibrational levels, which can be split into two categories, bound ($\mathcal{B}$) and predissociated ($\mathcal{P}$). The bound levels are the levels whose total energy is less than the dissociation energy ($9.75eV$) of nitrogen molecule in its electronic ground state. The predissociated levels are the levels whose energy is higher than the dissociation energy relative to the

first rovibrational energy, but lower than the rotational dependent centrifugal barrier [12].
A simulation with all the 9390 different levels would have a huge computational cost. In order to reduce the computational cost coarse-grained models are developed. The reduction strategy that chosen for this project is the Uniform Rovibrational Collisional bin model (URVC) [16]. The rovibrational energy levels are sorted in an increasing energy levels ladder. Then, this ladder is divided into two parts, the first one containing only the bound levels and the second one only the predissociated levels. Lastly, each of these two regions is divided with equal energy spacing:

$$\Delta E_{\mathcal{B}} = \frac{2E_{fN}}{\mathcal{N}_{\mathcal{B}}}, \quad \Delta E_{\mathcal{P}} = \frac{E_{max} - 2E_{fN}}{\mathcal{N}_{\mathcal{P}}} \tag{1}$$

where E_{fN} is the formation energy of N and E_{max} the energy of the last energy level of N_2. $\mathcal{N}_{\mathcal{B}}$ and $\mathcal{N}_{\mathcal{P}}$ are the number of bound and predissociated bins, which can be chosen freely. The higher their number the better is the fidelity of the model. Here we have chosen $\mathcal{N}_{\mathcal{B}} = 7$ and $\mathcal{N}_{\mathcal{P}} = 3$. A sensitivity analysis has been performed in [18] and it was shown that no big effect on the heat flux was observed going from 10 bins to 100 bins. The population distribution, n_l, of the energy levels contained in each bin is chosen to be uniform:

$$n_l = \frac{g_l \sum_i n_i}{\sum_i g_i} \tag{2}$$

where g_i is the degeneracy of level i and n_i its population. The number density n_k of each bin is $\sum_l n_l$; its degeneracy g_k is $\sum_l g_l$. The average energy of bin k is equal to:

$$\bar{E}_k = \frac{1}{\sum_l g_l} \sum_i g_i E_i \tag{3}$$

where E_i is the internal energy of the i^{th} level. Alternative strategies of model reduction can be found in [15, 18]. The advantages of the URVC model are the simple implementation, the fact that the average energy of the bins is not a function of the thermodynamic state and good quality of the results, especially at high temperatures. A non equal energy spacing for the bins might also improve the quality at lower temperatures. The main disadvantage of this model is that it cannot reach Boltzmann equilibrium at a fine-grain level.
As a post processing result an internal temperature (T_{int}) has been defined by solving the following equation:

$$\frac{\sum_k n_k \bar{E}_k}{n_{N_2}} = \frac{\sum_k \bar{E}_k g_k \exp(\bar{E}_k / k_B T_{int})}{\sum_k g_k \exp(\bar{E}_k / k_B T_{int})} \tag{4}$$

Physically, it represents the temperature that would exist in the flow field if the internal energy levels of N_2 were populated in a Boltzmann way, with the mixture having the same amount of internal energy.

2.2. Reaction Mechanism

In a $(N(^1S_u) - N_2(^1\Sigma_g^+))$ mixture two kind of interactions can exist. The first one is the collision between nitrogen atoms and molecules, the second one the collision between nitrogen molecules. In the present model only the first category of collisions has been considered. The second one has not been taken into account because only a portion of all the possible transitions rates are currently available [20].
Spontaneous dissociation was also assumed to be negligible [18]. The total number of reactions that are needed to describe the possible transitions from one rovibrational level to any other or to dissociated nitrogen, with the third body being a nitrogen atom, is of the order of $2 \cdot 10^7$. The reactions belong to two different categories, the third body dissociation reaction and the inelastic transitions reaction between rovibrational levels:

$$N_2(l) + N \underset{k_l^{rec}}{\overset{k_l^{dis}}{\rightleftharpoons}} N + N + N \tag{5}$$

$$N_2(l) + N \underset{k_{l'\to l}^{in}}{\overset{k_{l\to l'}^{in}}{\rightleftharpoons}} N_2(l') + N \tag{6}$$

The forward reaction rates are computed with the quasi-classical trajectory (QCT) method, using potentials calculated from ab-initio quantum mechanics computations [12]. The backward reaction rates are computed with the microreversibility principle.
For the URVC bin model the same reaction categories apply, but on each single bin. The forward reaction rates of bin k are obtained from the formulas:

$$k_k^{dis} = \frac{1}{g_k} \sum_l g_l k_l^{dis} \quad k_{k\to k'}^{in} = \frac{1}{g_k} \sum_{k,l} g_l k_{l\to l'}^{in} \tag{7}$$

The backward reaction rates are not connected through the micro-reversibility principle to the forward ones; they are computed using the equilibrium constant which is obtained by minimizing the Gibbs free energy of the bins. In this way equilibrium is obtained at a bin level. In order to correctly compute the minimum Gibbs free energy, even without electronic energy, the degeneracy of the first electronic level of N is required, that for the state-to-state model is equal to 12.

3. GOVERNING EQUATIONS

The dynamical evolution of the bins is governed by the Navier-Stokes equations:

$$\frac{\partial \rho_i}{\partial t} + \nabla \cdot (\rho_i \mathbf{u} + \mathbf{j}_i) = \dot{\omega}_i, \tag{8}$$

$$\frac{\partial \rho \mathbf{u}}{\partial t} + \nabla \cdot (\rho \mathbf{u} \otimes \mathbf{u} + p\underline{\underline{I}} + \underline{\underline{\tau}}) = \mathbf{0}, \tag{9}$$

$$\frac{\partial \rho E}{\partial t} + \nabla \cdot (\rho \mathbf{u} H + \underline{\underline{\tau}}\mathbf{u} + \mathbf{q}) = 0. \tag{10}$$

ρ_i is the partial density of bin i, $\rho\mathbf{u}$ and ρE are momentum and total energy of the whole mixture. $\mathbf{j}_i$ is the diffusion flux and $\dot{\omega}_i$ is the chemical production/destruction term of bin i. The identity matrix is symbolized with $\underline{\underline{I}}$, p is the mixture pressure, $\underline{\underline{\tau}}$ is the stress tensor and $\mathbf{q}$ is the heat flux. If Eqs. 8 are summed up over all the species

in the mixture, the total continuity equation will be obtained, since $\sum_i \rho_i = \rho$. For the state-to-state approach, one distinct continuity equation for each bin is solved. Each bin is supposed to behave as a perfect gas.

3.1. Transport Properties

In order to close the Navier-Stokes equations (Sec. 3) that govern the bins dynamic, expressions for diffusion flux, stress tensor and heat flux should be obtained. The transport properties are computed using the *Mutation++* library, developed by Scoggins and Magin [24] at the von Karman Institute for Fluid Dynamics. In the computation of the transport properties it is assumed that the elastic collisions cross sections are the same for all internal quantum states and inelastic collisions have no influence. The diffusion flux is computed with the Stefan-Maxwell equations (there is one of these equations for each bin):

$$\frac{M}{\rho}\sum_k \left(\frac{x_i \mathbf{j_k}}{M_k \mathcal{D}_{ik}} - \frac{x_k \mathbf{j_i}}{M_i \mathcal{D}_{ik}}\right) = \nabla x_i \qquad (11)$$

where ∇x_i is mole fraction gradient of bin i. $\mathcal{D}_{ik}$ is the binary diffusion coefficient.
Stress tensor reads classically:

$$\underline{\underline{\tau}} = -\mu[\nabla \mathbf{u} + (\nabla \mathbf{u})^T - \frac{2}{3}\nabla \cdot \mathbf{u}\underline{\underline{I}}], \qquad (12)$$

where μ is the shear viscosity.
Heat flux reads:

$$\mathbf{q} = -\lambda \nabla T + \sum_i h_i \mathbf{j}_i \qquad (13)$$

where λ is the thermal conductivity associated with the translational temperature T of the gas species and the second term is the diffusive heat flux, which will be referred as q_{diff}.

3.2. Numerical solution

The above formulation has still a high computational cost because of the subdivision into bins. For this reason a special formulation of the Navier-Stokes equations, called dimensionally reduced Navier-Stokes equations (DRNSE) [13], that simulates the flow field only on the stagnation line of the re-entry vehicle is solved. The Navier-Stokes equations are written in spherical (r, θ, ϕ) coordinates. The flow is assumed to be axisymmetric and therefore $u_\phi = 0$ and $\partial/\partial\phi = 0$. The symmetry of the flow implies that u_r, p, T and ρ_i are symmetric (cosine) with respect to the stagnation line axis (located at $\theta = 0$) and u_θ is antisymmetric (sine) with respect to it. Furthermore, the Newtonian theory for pressure distribution of hypersonic flows is assumed. Finally, by taking the limit of $\theta \to 0$ the DRNSE equations [13] are obtained. The DRNSE system of equations is solved using the finite volume method in space, with an implicit Backward Euler method in time [11]. Detailed information about the numerical method can be found in [18].

4. CATALYTIC WALL

The surface of the thermal protection system can act as a catalyzer with respect to the gas mixture chemical species that impinge on it. If this is the case, the recombination of dissociated species is promoted and the chemical energy released increases the heat load of the vehicle. In order to model this phenomenon, a correct boundary condition should be imposed at the wall surface for the mixture's chemical species. For a catalytic wall at a steady state, the mass of each species produced or destroyed by surface reactions should be equal to the diffusion flux of the species at the wall. Hence:

$$\mathbf{j}_i \cdot \mathbf{n}_w = \dot{w}_{i,cat} \qquad (14)$$

where $\mathbf{n}_w$ is the unit vector normal to the surface and $\dot{w}_{i,cat}$ is the mass of species i produced or destroyed per unit of area and unit time. The right hand side is modeled using a phenomenological approach, the γ model, widely used in the aero-thermodynamics community [4, 7]. The recombination probability γ_i is defined as:

$$\gamma_i = \frac{M_{i,rec}}{M_i^{\downarrow}}, \qquad (15)$$

where $M_i^{\downarrow}$ is the flux of species i impinging the surface and $M_{i,rec}$ is the flux of species recombining at the surface. A fully catalytic wall has γ_i equal to 1, which means that all the particles of species i impinging the surface recombine at the wall. γ_i equal to 0 means that no reaction takes place and corresponds to a non-catalytic wall. Anything between these two extreme cases is a partially catalytic wall. Knowing the probability γ_i, the right hand side of Eq. 14 is equal to [4]:

$$\dot{w}_{i,cat} = \gamma_i m_i M_i^{\downarrow} \qquad (16)$$

When the translational energy modes of gas species close to the wall have a Maxwellian distribution function and there is no temperature slip, the impinging flux, $M_i^{\downarrow}$, is equal to [4]:

$$M_i^{\downarrow} = n_i \sqrt{\frac{kT_w}{2\pi m_i}} \qquad (17)$$

where T_w is the wall temperature. For the state-to-state model specific wall recombination reactions are considered for every different rovibrational bin, each one with their own recombination probabilities γ_i:

$$N + N \xrightarrow{\gamma_i} N_2(i). \qquad (18)$$

Since in literature there are no available values for γ_i, three cases are considered. In the first case γ_i is assumed to be equal for every bin. γ_i is obtained by dividing a global recombination probability γ by the number of bins considered in the model. For this contribution, $\gamma = 0.01$ and because we consider 10 bins $\gamma_i = 0.001$. This case will be referred as the equiprobable catalytic case. In the second case, it is assumed that recombination occurs only in the lower energy bin, which means that $\gamma_{i=1} = 0.01$

and the others are equal to 0. This case is called the lower catalytic case. In the third case recombination occurs only to the highest energy bin. This will be the upper catalytic case.
As a concluding remark, it should be mentioned that the purpose of the paper was not to find a rigorous value for recombination probabilities. The aim was to check how the heat flux is affected in each case. In the future, there are plans to extract from a finite rate chemistry and a dynamical Monte Carlo approach more accurate recombination probabilities γ_i and couple them with the bin model [8, 25, 9].

4.1. Accommodation Coefficient

The recombination of atoms at the surface releases their chemical energy. Nonetheless, not all of this energy should transferred to the surface. Some of it may be saved within the created molecule as internal energy (rotational, vibrational or electronic). One of the aims of using state-to-state models for catalysis is to determine how much of this energy is released to the wall and how much is saved as energy of the molecules. A suitable parameter, the chemical energy accommodation coefficient β, is introduced [10]:

$$\beta = \frac{q_{diff}}{\sum_i \dot{\omega}_{i,cat} \Delta H_{i,R}(T_{wall})}, \tag{19}$$

where q_{diff} is the diffusive heat flux and $\Delta H_{i,R}(T_{wall})$ is energy released by the recombination reaction that involves bin i at thermal equilibrium. The β coefficient is non-dimensional and can take values between 0 and 1. $\beta = 0$ means that none of the energy released during the catalytic recombination is transferred to the wall and $\beta = 1$ means the opposite.
Researchers often use the product of β and γ coefficients defining an overall effective catalytic probability, γ_{eff}, in order to characterize the catalytic efficiency derived from experiments [5]. In this paper the chemical energy accommodation coefficient is explicitly determined. Similar approaches for the determination of the accommodation coefficient can be found in [3].

5. RESULTS

The flow on the stagnation line around a spherical blunt body of radius $r = 0.4\,m$ is studied. The free stream pressure is equal to $p_\infty = 44\,Pa$, the temperature is $T = 300\,K$ and the free stream velocity is equal to $10000\,m/s$ ($M = 28.33$). Because, only $N_2 - N$ collisions are considered, the free stream is seeded with 2.8% per mole of atomic nitrogen. The wall is considered in equilibrium with temperature equal to $2000K$. This temperature is relatively high for catalytic studies, nonetheless it has has been chosen for validation purposes in order to have a test case consistent previous ones [18, 19].
In Fig. 1 the temperature profiles for the non-catalytic

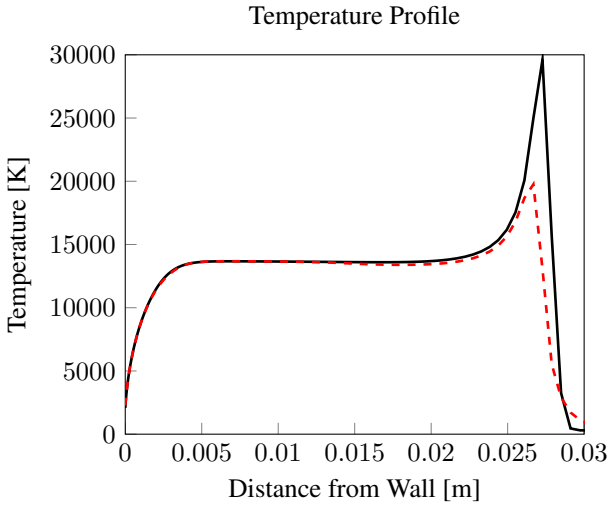

Figure 1. State-to-state simulations for N in for the non-catalytic case. Temperature profile along the stagnation line. ***(unbroken line)****: Translational temperature;* ***(dashed line)****: Internal temperature.*

case along the stagnation line are presented; translational and the internal (see Eq. 4) temperatures are shown. The free stream is not in thermal equilibrium, because at low temperatures the URVC model stores an excess of energy in the first bin; this effect fades away once the temperature increases. An area of strong thermal non-equilibrium is observed across the shock wave. At a distance of $x = 0.02\,m$ from the wall the two temperatures becomes practically equal. The two temperature are very close to each other inside the boundary layer, except at the wall $x = 0\,m$.
The internal energy bins population inside the boundary layer, close to the wall, is plotted in Figs. 2 and 3 in terms of their molar fractions divided by the bin degeneracy. In Fig. 2-top the non-catalytic case is shown. Inside the boundary layer, up to a distance from the wall equal to $x = 4 \cdot 10^{-4}\,m$, the energy levels have a Boltzmann distribution, as it is seen by the straight line in the logarithmic plot, which changes its slope because of the decrease in temperature due to the influence of the wall. At $x = 2 \cdot 10^{-4}\,m$ the Boltzmann character starts to be lost; the non predissociated higher energy states get more and more populated, while the predissociated states are depleted. This effect is maximized at the wall.
Fig. 2-bottom shows the distribution of internal energy bins for the lower catalytic case. The behaviour is similar to the non-catalytic case, except that the first bin is overpopulated, because the wall promotes recombination of nitrogen atoms into molecules belonging to the first bin.
Fig. 3 shows the distribution of the internal energy bin for the, equiprobable (top) and upper catalytic (bottom) cases. The two cases show a similar trend. Up to a distance of the order of $x = 2 \cdot 10^{-4}\,m$ from the wall the levels are populated with a Boltzmann distribution. Very close to the wall the Boltzmann distribution does not hold any more and the higher energy bins are overpopulated in both cases; catalysis promotes thermal non-equilibrium

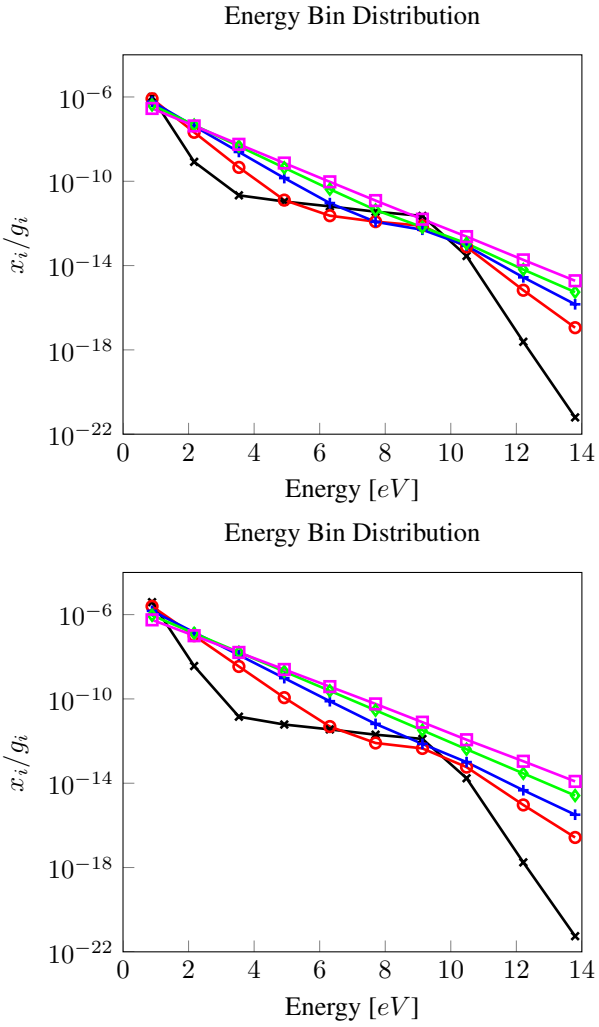

*Figure 2. Distribution of the internal energy bins close to the surface for the non-catalytic (*top*) and lower (*bottom*) case. (**x**: $x = 0\,m$; **o**: $x = 2{\cdot}10^{-4}\,m$; **+**: $x = 4{\cdot}10^{-4}\,m$; **diamond**: $x = 6 \cdot 10^{-4}\,m$; **square**: $x = 8 \cdot 10^{-4}\,m$).*

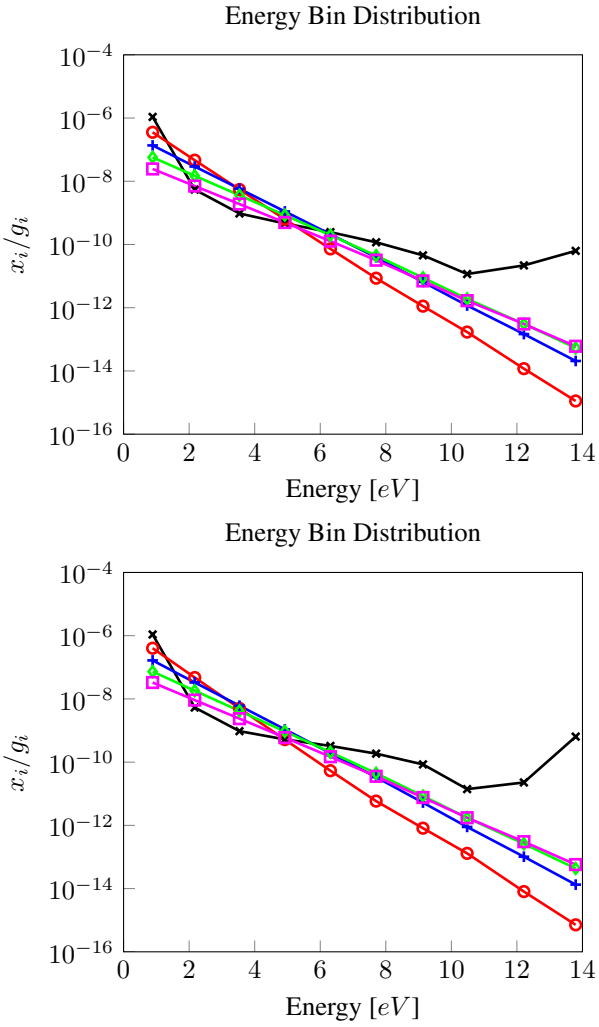

*Figure 3. Distribution of the internal energy bins close to the surface for the equiprobable (*top*) and upper (*bottom*) catalytic case. (**x**: $x = 0\,m$; **o**: $x = 2 \cdot 10^{-4}\,m$; **+**: $x = 4 \cdot 10^{-4}\,m$; **diamond**: $x = 6 \cdot 10^{-4}\,m$; **square**: $x = 8 \cdot 10^{-4}\,m$).*

at the wall. For the sake of comparison the distributions of energy bins at the wall, for all the four cases, are plotted together in Fig. 4.

Fig. 5 depicts the molar fraction of N along the stagnation line for the four cases. In the non-catalytic case (*unbroken line*) the recombination is due only to the recombination reactions in the gas phase. The recombination predicted by the present model is lower compared to the one predicted by the Park model [18, 23]. In the lower catalytic case (*dotted-dashed line*) the nitrogen molar fraction is further reduced because of wall recombination. This does not happen for the equiprobable and upper catalytic cases, where the populations of the N atoms are higher. This is mainly due to two combined effects. First of all, it can be seen in Fig. 5 that the boundary layer is less thick in the equal and upper catalytic cases. This leads to a reduced recombination, because of the less time available for the reactions. Secondly, since in these two cases nitrogen molecules are preferentially formed in high vibrational states, they are much more likely to dissociate after desorption and to release their internal energy into translational one, a phenomenon known as quenching. This effect can be inferred from the temperature profiles inside the boundary layer. Fig. 6 shows the translational and internal temperature profiles in the boundary layer for the four cases. The profiles of the non-catalytic and lower catalytic cases are very similar and the same happens for the equally and fully catalytic case. The translational temperature gradient increases going from non-catalytic to the upper catalytic case, because highly excited desorbed molecules transfer their internal energy to translational one. In Fig. 6-bottom the internal temperatures of the flow field are presented. In the non-catalytic case the internal temperature at the wall is equal to $2252\,K$ which is higher than the imposed translational temperature. Therefore, the assumption of thermal equilibrium at the wall is not valid and this effect

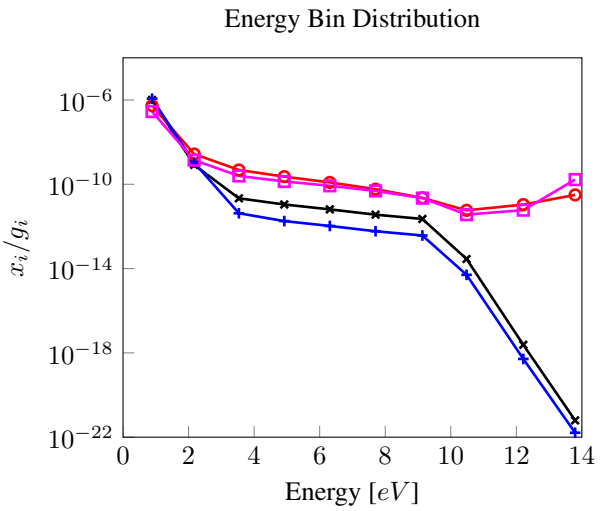

Figure 4. Comparison of distributions of internal energy bins for the four catalytic cases. ***x****: Non-catalytic case;* ***+****: Lower catalytic case;* ***o****: Equiprobable catalytic case;* ***square****: Upper catalytic case.*

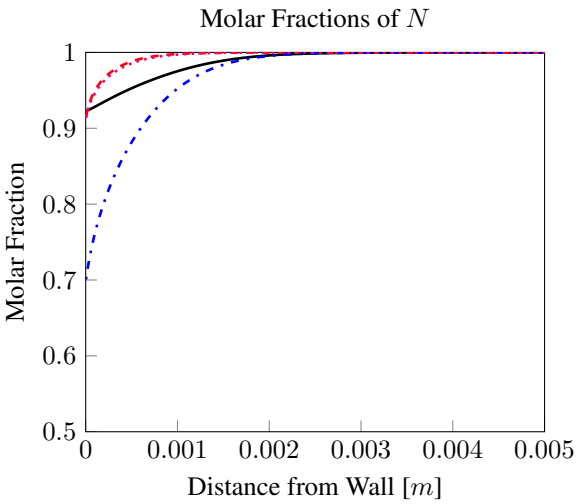

Figure 5. Comparison of N molar fraction for the four cases. **unbroken line***: Non-catalytic case;* **dotted-dashed line***: Lower catalytic case;* **dashed line***: Equiprobable catalytic case;* **dotted line***: Upper catalytic case.*

should be taken into consideration in multi-temperature simulations. As the wall catalycity increases the internal temperature increases too and it reaches the highest value of $4384\,K$ for the upper catalytic case. These results are consistent with similar ones available in literature [18].

Heat fluxes are shown in Tab. 1. The wall heat flux for the non-catalytic case is $3.02\,MW/m^2$; the diffusive heat flux contribution is zero since it is a non-catalytic wall. In the catalytic cases heat flux is the sum of the conductive contribution $\mathbf{q_{con}} = -\lambda\nabla T$ and the diffusive one $\mathbf{q_{con}} = \sum_i h_i$. For the lower catalytic case the conductive heat flux increase due to the increase in the slope of the temperature. The diffusive heat flux is also high and of the order of magnitude of the conductive heat flux. As we impose equiprobable recombination or recombination to the upper energy bin the heat flux greatly increases due mainly to the contribution of the conductive heat flux. The diffusive heat flux though decreases, because, as already mentioned in the comments to Fig. 5, there is little net recombination of nitrogen atoms. The results shown in this paragraph for our nitrogen state-to-state model agree qualitatively with the ones obtained for a vibrational specific oxygen model in [2, 14].

The values of the β coefficient computed accordingly to Eq. 19 are shown in Tab. 2. In the non-catalytic case the β coefficient cannot be defined. In the catalytic cases, as already explained, β can take values between 0 and 1. In the lower catalytic case only a small part of the recombination energy is transferred to the internal energy of the desorbed N_2 molecule. Most of the energy is therefore transferred to the surface and for this reason we have $\beta = 0.9325$, very close to one. This is the maximum value attained by the β coefficient. In the upper catalytic case, where all of the N atoms recombine into the highest energy bin of N_2, the β coefficient is equal to 0.1005 meaning that very small part of the recombination energy is directly transferred to the wall. The equiprobable catalytic case stays in between with $\beta = 0.5757$. In the last two cases, even though only a small part of the recombination energy is directly transferred to the surface, the heat flux increases substantially, because the quenching phenomenon enhances the conductive part of the heat flux. Therefore, even though the β coefficient has an interesting physical meaning, it cannot be used as an accurate indicator for the total heat flux transferred to the wall, but only as an indicator of the diffusive (reactive) portion of heat flux directly transferred to the wall.

Table 1. Heat flux $[MW/m^2]$ for the URVC bin model.

	$\mathbf{q_{total}}$	$\mathbf{q_{con}}$	$\mathbf{q_{diff}}$
Non-catalytic	3.02	3.02	–
Lower catalytic	7.48	3.85	3.63
Equal catalytic	17.58	15.07	2.51
Upper catalytic	15.3	14.87	0.43

Table 2. β coefficient and T_{int} $[K]$ for the URVC bin model

	β	T_{int}
Non-catalytic	–	2252
Lower catalytic	0.9325	2159
Equal catalytic	0.5757	3917
Upper catalytic	0.1005	4834

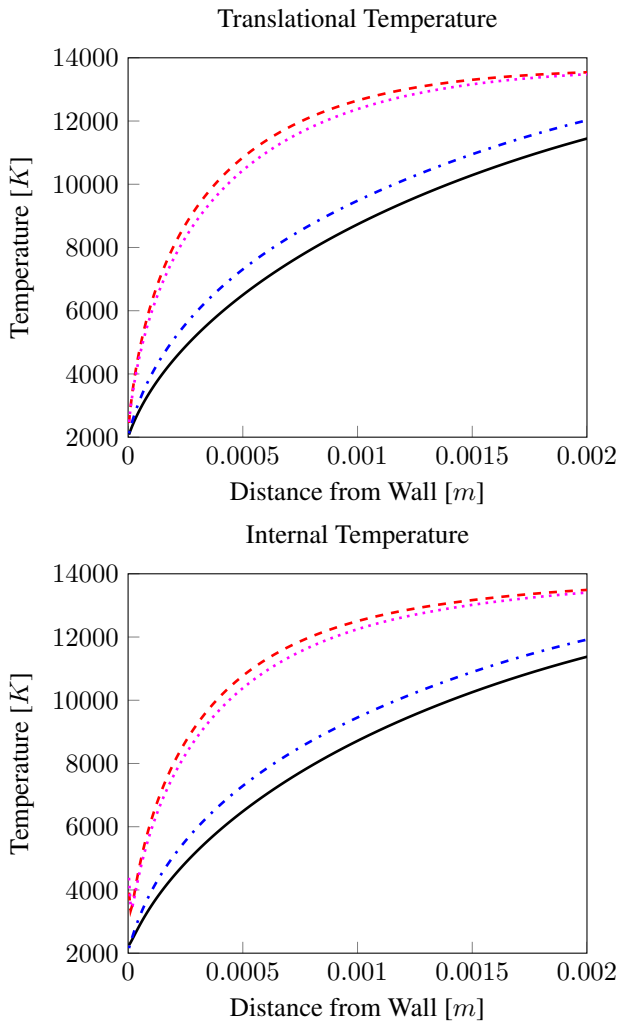

Figure 6. Comparison of the translational and internal temperature profiles for the four cases. ***(unbroken line)****: Non-catalytic case;* ***(dotted-dashed line)****: Lower catalytic case;* ***(dashed line)****: Equiprobable catalytic case;* ***(dotted line)****: Upper catalytic case.*

6. CONCLUSIONS

In this paper the joint effects of thermal non-equilibrium and catalysis have been studied on the stagnation line flow field of a re-entry body. The Uniform Rovibrational Collisional coarse-grained model of nitrogen has been used. The coarse-grained model is based on an ab-initio rovibrational nitrogen model developed at NASA Ames research center. The gamma model has been used in order to simulate the catalytic properties of the re-entry body thermal protection system and it has been extended in order to account for the rovibrational model. The flow field has been modeled by solving the Navier-Stokes equations using an implicit Finite Volume method.
Heat flux is strongly affected by the mutual interaction of catalysis and thermal non-equilibrium. The diffusive heat flux decrease when catalysis acts only on the higher energy levels, with a specular decrease of the β coefficient. Nonetheless the conductive heat flux is strongly enhanced by the quenching phenomenon, leading, in the end, to a net increase of the overall heat flux. These results are in agreement with previous literature data.
As a future work, the Boltzmann rovibrational collisional model can be used in order to remove some of the weak points of the Uniform rovibrational collisional model. $N_2 - N_2$ collisions should also be included, as well as electronic energy levels beyond the ground one. Extension to a full air mixture including the O_2 and NO molecules would be also of interest, making the comparison to experimental results easier. As far as the treatment of the wall is concerned, treating catalysis with a microkinetic model is in view. The latter model can be coupled directly with a flow solver or used as a test bench for obtaining more accurate values for the catalytic recombination probability γ. Validation of the results is also necessary by comparing the simulations with experimental results on catalysis, performed at von Karman Institute or by other experimental teams.

ACKNOWLEDGEMENTS

The authors are grateful to James B. Scoggins for his time and support concerning the usage and further development of the *Mutation++* library, to Erik Torres for his tools for the reduction of the full NASA model into the Uniform Rovibrational Collisional one and to Alessandro Munafò for the stagnation line code. Research of G. B. C. and T. E. M. is sponsored by the European Research Council Starting Grant #2549354.

REFERENCES

1. J.D. Anderson. *Hypersonic and High-Temperature Gas Dynamics*. AIAA Education Series. American Institute of Aeronautics and Astronautics, 2006.

2. I. Armenise, M. Capitelli, Cl. Gorse and M. Rutigliano. Nonequilibrium vibrational kinetics of an O_2/O mixture hitting a catalytic surface. *Journal of Spacecraft and Rockets*, 37:3:318–323, 2000.

3. M. Balat-Pichelin, V.L. Kovalev, A.F. Kolesnikov and A.A. Krupnov. Effect of the incomplete accommodation of the heterogeneous recombination energy on heat fluxes to a quartz surface. *Fluid Dynamics*, 43(5):830–838, 2008.

4. P. F. Barbante. *Accurate and Efficient Modeling of High Temperature Nonequilibrium Air Flows*. PhD thesis, Université Libre de Bruxelles, 2001.

5. O. Chazot. Experimental studies on hypersonic stagnation point chemical environment. *RTO-EN-AVT-142 von Karman Institute Lecture Series: Experiment, Model and Simulation of Gas-Surface Interactions for Reactive Flows in Hypersonic Flights*, 2007.

6. I. Chorkendorff and J.W. Niemantsverdriet. *Concepts of Modern Catalysis and Kinetics*. Wiley, 2006.

7. R. Goulard. On catalytic recombination rates in hypersonic stagnation heat transfer. *Jet Propulsion*, 28:737–745, 1958.

8. V. Guerra. Analytical model of heterogeneous atomic recombination of silica-like surfaces. *IEEE Transaction on plasma science*, 5:35, 2007.

9. V. Guerra and J. Loureiro. Dynamical Monte Carlo simulation of surface atomic recombination. *Plasma Sources Sci. Technol.*, 13:85, 2004.

10. B. Halpern and D. E. Rosner. Chemical energy accommodation at catalyst surfaces. Flow reactor studies of the association of nitrogen atoms on metals at high temperatures. *Transactions of the Faraday Society*, 74:1883–1912, 1978.

11. C. Hirsch. *Numerical Computation of Internal and External Flows: The Fundamentals of Computational Fluid Dynamics*. Elsevier Science, 2007.

12. R. Jaffe, W. Schwenke and. G. Chaban and W. Huo. Vibrational and rotational excitation and relaxation of nitrogen from accurate theoretical calculations. *AIAA paper 2008-1208. 46th AIAA Aerospace Sciences Meeting and Exhibit, Reno, NV*, pages 9,49,50,54, 2008.

13. A. Klomfass and S. Müller. A quasi-one dimensional approach for hypersonic stagnation-point flows. Technical report, RWTH Aachen, 1996.

14. E. Kustova, E. Nagnibeda, I. Armenise and M. Capitelli. Nonequilibrium kinetics and heat transfer in O_2/O mixtures near catalytic surfaces. *Journal of Thermophysics and Heat Transfer*, 16:2:238–244, 2002.

15. T. E. Magin, M. Panesi, A. Bourdon, R. Jaffe and D. Schwenke. Internal energy excitation and dissociation of molecular nitrogen in a compressing flow. *AIAA 2009-3837. 41st AIAA Thermophysics Conference, San Antonio, Texas*, 2009.

16. T.E. Magin, M. Panesi, A. Bourdon, R. L. Jaffe and D. W. Schwenke. Coarse-grain model for internal energy excitation and dissociation of molecular nitrogen. *Chemical Physics*, 398(0):90 – 95, 2012.

17. M.F. Modest. *Radiative Heat Transfer*. Chemical, Petrochemical & Process. Academic Press, 2003.

18. A. Munafò. *Multi-Scale models and Computational methods for Aerothermodynamics*. PhD thesis, Ecole Central Paris, 2014.

19. A. Munafò and T. E. Magin. Modeling of stagnation-line nonequilibrium flows by means of quantum based collisional models. *Physics of Fluids*, 26(9):–, 2014.

20. M. Panesi, R. Jaffe and D. Schwenke. Energy transfer study of N2-N2 interactions by using rovibrational state-to-state model. *AIAA 2013-3147. 44st AIAA Thermophysics Conference*, 2013.

21. M. Panesi. *Physical models for nonequilibrium plasma flow simulations at high speed re-entry conditions*. PhD thesis, Università degli Studi di Pisa, 2009.

22. C. Park. *Nonequilibrium Hypersonic Aerothermodynamics*. Wiley, 1990.

23. C. Park. Review of chemical-kinetic problems of future NASA missions. I: - earth entries. *Journal of Thermophysics and Heat Transfer*, 7-3:385–398, 1993.

24. J. B. Scoggins and T. E. Magin Development of Mutation^{++}: MUlticomponent Thermodynamics And Transport properties for Ionized Plasmas written in C++. *AIAA 2014-2966. 11th AIAA/ASME Joint Thermophysics and Heat Transfer Conference*, 2014.

25. C. Sorensen, P. Valentini and T. E.Schwartzentruber Uncertainty Analysis of Reaction Rates in a Finite-Rate Surface-Catalysis Model. *Journal of Thermophysics and Heat Transfer*, 26-3:407-416

26. J. Thoemel. *Surface catalysis in high enthalpy flows*. PhD thesis, RWTH Aachen, von Karman Institute for Fluid Dynamics, January 2013.